Preclinical Evaluation of ^{213}Bi- and ^{225}Ac-Labeled Low-Molecular-Weight Compounds for Radiopharmaceutical Therapy of Prostate Cancer

Sangeeta Ray Banerjee[1,2], Ala Lisok[1], Il Minn[1], Anders Josefsson[1], Vivek Kumar[1], Mary Brummet[1], Srikanth Boinapally[1], Cory Brayton[3], Ronnie C. Mease[1,2], George Sgouros[1], Robert F. Hobbs[1,4], Martin G. Pomper[1,2,4]

[1]*Russell H. Morgan Department of Radiology and Radiological Science, Johns Hopkins University School of Medicine, Baltimore, Maryland;* [2]*Sidney Kimmel Comprehensive Cancer Center, Johns Hopkins University School of Medicine, Baltimore, Maryland;* [3]*Department of Molecular and Comparative Pathobiology, Johns Hopkins University School of Medicine, Baltimore, Maryland; and* [4]*Department of Radiation Oncology, Johns Hopkins University School of Medicine, Baltimore, Maryland*

Prostate-specific membrane antigen (PSMA)–targeted radiopharmaceutical therapy is a new option for patients with advanced prostate cancer refractory to other treatments. Previously, we synthesized a β-particle–emitting low-molecular-weight compound, ^{177}Lu-L1 which demonstrated reduced off-target effects in a xenograft model of prostate cancer. Here, we leveraged that scaffold to synthesize α-particle–emitting analogs of L1, ^{213}Bi-L1 and ^{225}Ac-L1, to evaluate their safety and cell kill effect in PSMA-positive (+) xenograft models. **Methods:** The radiochemical synthesis, cell uptake, cell kill, and biodistribution of ^{213}Bi-L1 and ^{225}Ac-L1 were evaluated. The efficacy of ^{225}Ac-L1 was determined in human PSMA+ subcutaneous and micrometastatic models. Subacute toxicity at 8 wk and chronic toxicity at 1 y after administration were evaluated for ^{225}Ac-L1. The absorbed radiation dose of ^{225}Ac-L1 was determined using the biodistribution data and α-camera imaging. **Results:** ^{213}Bi- and ^{225}Ac-L1 demonstrated specific cell uptake and cell kill in PSMA+ cells. The biodistribution of ^{213}Bi-L1 and ^{225}Ac-L1 revealed specific uptake of radioactivity within PSMA+ lesions. Treatment studies of ^{225}Ac-L1 demonstrated activity-dependent, specific inhibition of tumor growth in the PSMA+ flank tumor model. ^{225}Ac-L1 also showed an increased survival benefit in the micrometastatic model compared with ^{177}Lu-L1. Activity-escalated acute and chronic toxicity studies of ^{225}Ac-L1 revealed off-target radiotoxicity, mainly in kidneys and liver. The estimated maximum tolerated activity was about 1 MBq/kg. α-Camera imaging of ^{225}Ac-L1 revealed high renal cortical accumulation at 2 h followed by fast clearance at 24 h. **Conclusion:** ^{225}Ac-L1 demonstrated activity-dependent efficacy with minimal treatment-related organ radiotoxicity. ^{225}Ac-L1 is a promising therapeutic for further clinical evaluation.

Key Words: prostate-specific membrane antigen (PSMA); α-particle; prostate carcinoma; long-term toxicity; murine

J Nucl Med 2021; 62:980–988
DOI: 10.2967/jnumed.120.256388

Prostate cancer is the most commonly diagnosed noncutaneous malignancy in men, with an estimated 31,620 deaths in 2020, a 5% increase from 2019 (*1*). Prostate-specific membrane antigen (PSMA) is a well-characterized tumor marker associated with metastatic castration-resistant prostate cancer (mCRPC), the most lethal form of the disease (*2–5*). Several PSMA-targeted approaches, including small-molecule (≤1,000 Da) ligands, peptides, and monoclonal antibodies, have been used for imaging and treating patients with mCRPC (*5–7*). In particular, PSMA-based radiopharmaceutical therapy (RPT) has appeared as a promising strategy for managing patients with mCRPC (*8*,*9*). Coupled with PSMA-based PET for patient selection and therapeutic monitoring, PSMA-based RPT is the treatment arm of a new radiotheranostic (*10*). To date, this approach has primarily applied agents that deliver therapeutic payloads using ^{177}Lu (half-life, 6.7 d), which emits β-particles of relatively low linear energy transfer (~0.2 keV/μm) (*11*). Along with other conventional β-particle strategies using ^{90}Y (*12*) or ^{131}I (*13*), α-particle–emitting radionuclides are being pursued to improve efficacy, leveraging short-range (50–100 μm), high–linear-energy-transfer radiation (~80 keV/μm) (*14–16*).

Among α-particle emitters, ^{225}Ac has received the most attention because of its 10-d physical half-life and high net emission energy of 27 MeV per decay (*17*,*18*). ^{225}Ac decays with the emission of 4 α-particles, generated by the daughter nuclides ^{221}Fr (half-life, 4.8 m), ^{217}At (half-life, 32 ms), ^{213}Bi (half-life, 45.6 min), and ^{213}Po (half-life, 4.2 μs) (*17*). Those α-particle–emitting daughters have also been identified as a source of unwanted off-target radiotoxicity (*19*). For example, ^{225}Ac-PSMA-617 produced remarkable imaging and prostate-specific antigen responses in patients with mCRPC refractory to most advanced therapies. However, it concurrently led to irreversible damage to the salivary glands, with attendant xerostomia (*14*,*20*). Additionally, although not an acute effect, renal toxicity may develop over time as more patients are treated more frequently and are studied over longer periods (*20*). Prospective clinical data addressing that important issue are lacking for PSMA α-RPT.

Several preclinical efficacy studies using small-molecule agents for PSMA α-RPT have appeared; however, only a few have addressed long-term and activity-limiting toxicity (*15*,*21–23*). Recently, we developed a series of such agents for ^{177}Lu-labeled PSMA-based RPT with the goal of reduced off-target toxicity using Glu-urea-Lys as the targeting moiety (*24*). A lead agent, ^{177}Lu-L1

Received Sep. 4, 2020; revision accepted Nov. 5, 2020.
For correspondence or reprints contact: Sangeeta Ray Banerjee, Johns Hopkins University, 1550 Orleans St., Cancer Research Building 2, Baltimore, MD 21287.
E-mail: sray9@jhmi.edu
Published online Nov. 27, 2020.

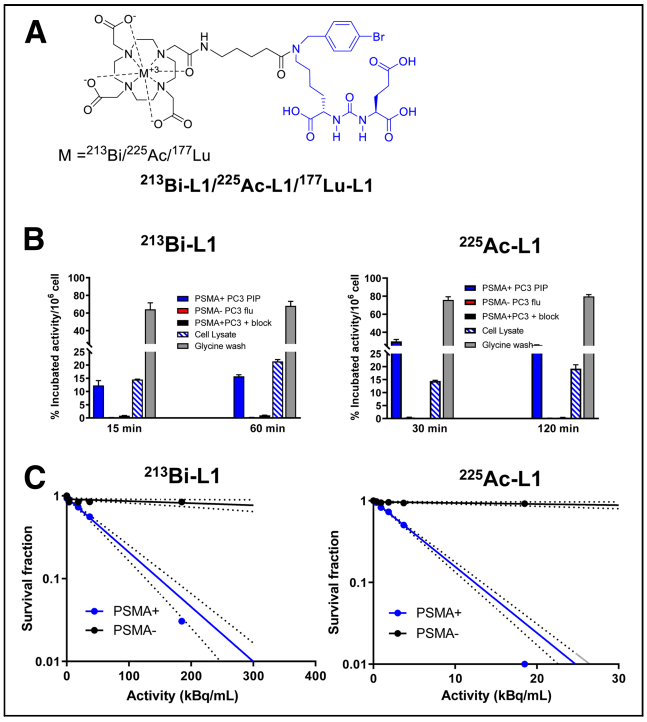

FIGURE 1. (A) Chemical structures of ^{213}Bi-L1 and ^{225}Ac-L1. (B and C) Cell uptake and internalization (B) (mean ± SD, n = 3) and cell kill effect (C) in PSMA+ PC3 PIP and PSMA− PC3 flu cells after 2 h of incubation at 37°C. Dashed line indicates 95% confidence limit for regression fit.

demonstrated minimal chronic radiotoxicity to most normal organs, including kidneys. As a next step, here we evaluated ^{225}Ac-L1 and ^{213}Bi-L1 (Fig. 1A) in relevant tumor models. Both compounds demonstrated specific uptake and efficacy in the PSMA-positive (+) PC3 flank tumor xenograft. We have further investigated ^{225}Ac-L1 for acute and chronic toxicity in immunocompetent mice and treatment efficacy in micrometastatic models. Compared with mice treated with ^{177}Lu-L1, tumor growth control was more effective in the group treated with ^{225}Ac-L1 in the micrometastatic model, with minimal off-target toxicity demonstrated.

MATERIALS AND METHODS

Reagents, Cell Lines, and Animal Models

^{213}Bi was eluted from a ^{225}Ac/^{213}Bi generator by following a standard operating procedure provided by the manufacturer, Oak Ridge National Laboratory. ^{225}Ac nitrate was also produced by Oak Ridge National Laboratory. Sublines of the androgen-independent PC3 human prostate cancer cell line, derived from advanced androgen-independent bone metastasis, were used (*25*). Six- to 8-wk-old male, nonobese diabetic/Shi-*scid* IL2rg^{null} (NSG; The Jackson Laboratory) mice (Johns Hopkins Animal Resources Core) were implanted subcutaneously with PSMA+ PC3 PIP (3×10^6) and PSMA-negative (−) PC3 flu cells (1×10^6 in 100 μL) in the forward right and left flanks, respectively (*15*,*25*). Immunocompetent CD-1 mice (Crl:CD1[ICR], 8–10 wk old; Charles River Laboratories) were used for the toxicity studies. Animal studies complied with the regulations of the Johns Hopkins Animal Care and Use Committee. Compound L1 was synthesized according to our recently reported method (*24*). Stable analogs—bismuth-L1, lanthanum-L1, and lutetium-L1—were prepared by following the method used for radiolabeling. The PSMA binding affinities of the stable analogs were determined using a fluorescence-based competitive binding assay (*25*).

Radiolabeling

Freshly eluted ^{213}Bi (18.5–30 MBq in 250 μL of a solution of 0.15 M KI in 0.1 M HCl) was added to a solution of 5–10 nmol (5–10 μL) of L1 (1 mM) and 5 μL of ascorbic acid (1.1 M), and the pH was adjusted to about 4–5 using 3 M NH_4OAc. The solution was heated in a radiochemistry microwave chamber at 90°C for 5 min at a power of 40 W (Resonance Instruments Inc.), and the resultant solution (~270 μL) was purified by high-performance liquid chromatography (HPLC) using a Phenomenex Luna C_{18} HPLC column (00G-4252-E0, 250 × 4.60 mm, 5 μm, 100 Å). Radiosynthesis of ^{225}Ac-L1 was also performed using microwave-assisted synthesis. In brief, to a solution of $^{225}Ac(NO_3)_3$ (7.4–11.1 MBq in 10–15 μL of 0.2 M HCl) was added 10 μL of ascorbic acid (1.1 M), about 10 nmol (10 μL) of L1 (1 mM), 50 μL of NH_4OAc (0.2 M), and 1–2 μL of NH_4OAc (5 M) to adjust to a pH of about 4. After microwave heating for 5 min, the solution was diluted with 200 μL of water and purified by HPLC. The flow rate was 1 mL/min, with water (0.1% trifluoroacetic acid) (A) and CH_3CN (0.1% trifluoroacetic acid) (B) as the eluting solvents. To ensure the highest purity, an isocratic solution of 79% A and 21% B was used to separate excess ligand from the radiolabeled compound.

Cell Uptake Study

Cell uptake studies were performed as previously described (*26*). Cells (1×10^6) were incubated with a 37 kBq/mL concentration of

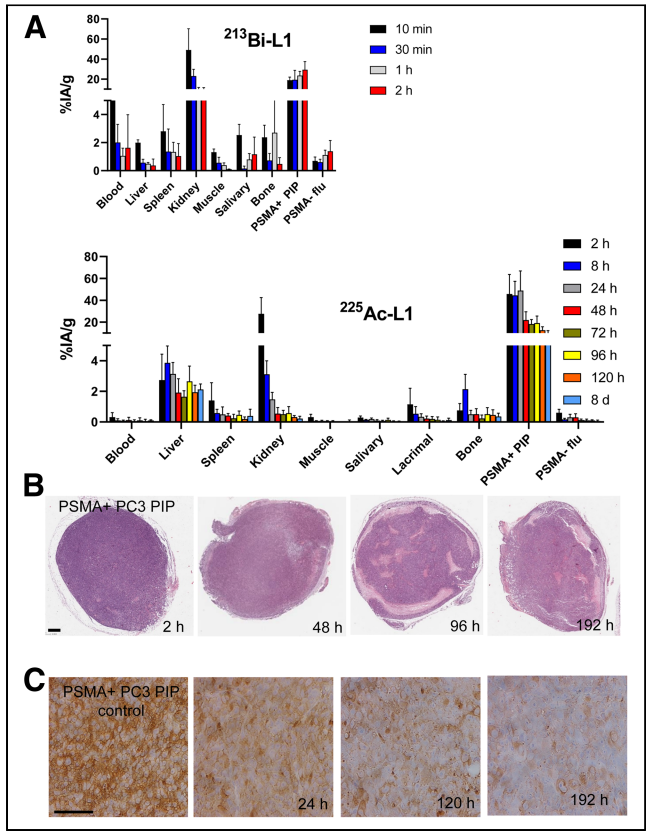

FIGURE 2. (A) Biodistribution data of ^{213}Bi-L1 and ^{225}Ac-L1 (percentage injected activity [%IA]/g, mean ± SD, n = 4). (B) Ex vivo staining of PSMA+ PC3 PIP tumor after administration of ^{225}Ac-L1 H&E (scale bar, 1.2 mm; ×2). (C) PSMA immunohistochemistry of PSMA+ PIP tumor (scale bar, 50 μm; ×20).

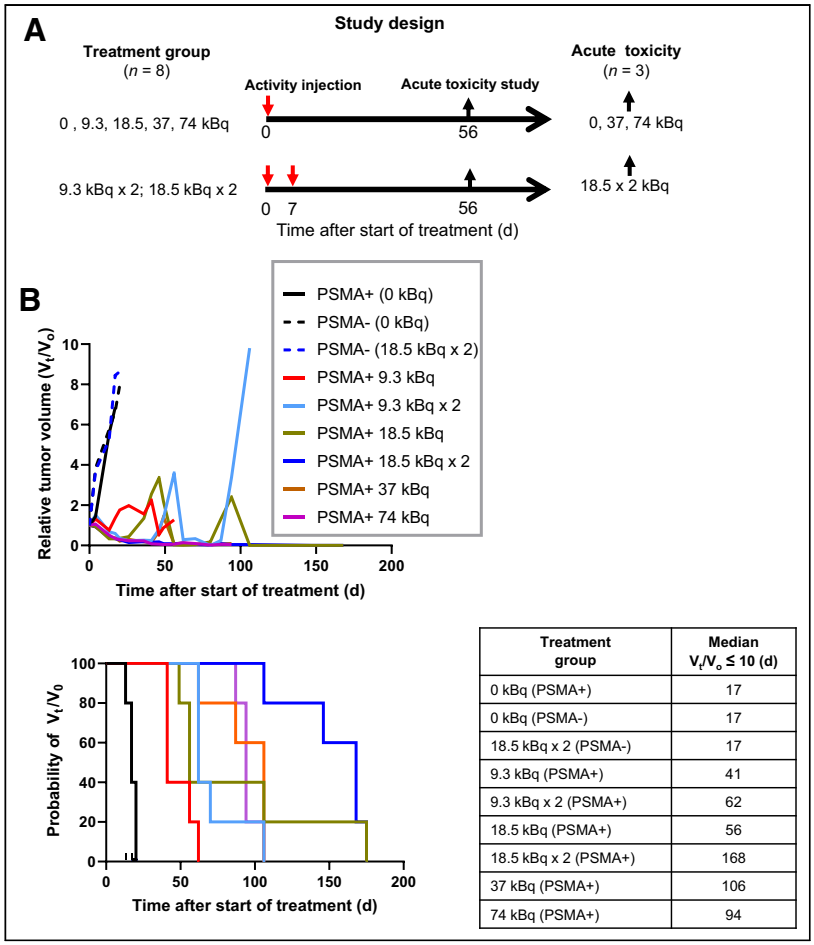

Treatment group	Median $V_t/V_o \leq 10$ (d)
0 kBq (PSMA+)	17
0 kBq (PSMA-)	17
18.5 kBq x 2 (PSMA-)	17
9.3 kBq (PSMA+)	41
9.3 kBq x 2 (PSMA+)	62
18.5 kBq (PSMA+)	56
18.5 kBq x 2 (PSMA+)	168
37 kBq (PSMA+)	106
74 kBq (PSMA+)	94

FIGURE 3. Activity-dependent RPT of ^{225}Ac-L1 in mice bearing either PSMA+ or PSMA− PC3 flu flank tumors after administration via tail-vein injection ($n = 5$). (A) Study design. (B) Relative tumor volume (V_t/V_o) (top); tumor growth curves relative to tumor volume at day 0 (set to 1). Kaplan–Meier curve illustrating time to grow $V_t/V_o \leq 10$ after treatment with ^{225}Ac-L1 or control (saline injection) (bottom).

each radiolabeled agent. To determine PSMA-binding specificity, cells were preblocked with the known PSMA inhibitor ZJ43 (*27*) to a final concentration of 10 μM. The obtained radioactivity values were converted into percentage incubated dose (%ID) per million cells.

Clonogenic Survival Assay

Cells (500–1,000) were seeded in 60-mm culture dishes. ^{225}Ac-L1 or ^{213}Bi-L1 was diluted in a prewarmed medium at different concentrations (0.04–74 kBq/mL for ^{225}Ac-L1 and 0.37–185 kBq/mL for ^{213}Bi-L1) and incubated with the cells for 2 h. The radiolabeled compound was replaced with fresh medium, and cells were incubated for 2 wk or until colonies had at least 50 cells. The colonies were stained with crystal violet and counted, and the surviving fraction was normalized to the control plating efficiency (*28*). A_0 (activity to reduce survival to 37%) and the 95% confidence limits of the regression fit were determined.

In Vivo Experiments

In vivo experiments (experiments 1–10) are summarized in Supplemental Table 1, along with the relevant information (supplemental materials are available at http://jnm.snmjournals.org).

Biodistribution. Biodistribution (Supplemental Tables 2–4) was determined according to our previously reported method (*25*). Mice were injected via the tail vein with ^{213}Bi-L1 (185 kBq) or ^{225}Ac-L1 (18.5 kBq) (experiments 1–3). ^{225}Ac in each organ was counted at 24 h after the sacrifice time to ensure complete secular equilibrium and using the ^{213}Bi energy window of 400–480 keV. Tissues were collected for histology at different time points. Tumor sections were stained with hematoxylin and eosin (H&E) using a standard protocol. Immunohistochemical staining was done as previously described by us (*24*) with an antihuman PSMA antibody (clone 3E6, M3620; Dako).

To determine the amount of free in vivo–generated ^{213}Bi from ^{225}Ac, the kidneys and PSMA+ tumor were counted immediately after sacrifice, repeatedly, using 1-min measurement intervals at the 400- to 480-keV energy window for ^{213}Bi for 5 h after sacrifice (experiment 4). A biexponential expression was fitted to the decay curves obtained to determine the equilibrium ^{225}Ac and free in vivo–generated ^{213}Bi at the time of sacrifice. Differences in ^{213}Bi radioactivity at the time of sacrifice and the levels from the equilibrium of ^{225}Ac reflect clearance or accumulation of ^{213}Bi. The time–activity curves of free ^{213}Bi were then constructed with free ^{213}Bi activities at multiple sacrifice time points.

Dosimetry and α-Camera Imaging. Absorbed dose coefficients (ADCs) for normal tissue and tumor were estimated for ^{225}Ac-L1 after accounting for the α-radiation deposited locally within the mouse according to an established method (*29*). Only α-particle emission was considered in the calculations. It was assumed to be deposited locally with the absorbed fraction, $\varphi = 1$, for both the parent ^{225}Ac and all radioactive daughters except in the kidneys, for which absorbed dose from additional free ^{213}Bi was tabulated. Potential human ADCs were estimated using a standard mouse-to-human conversion formula for time-integrated activities (*30*), which were then input to OLINDA/EXM, version 1.0 (*31*).

Digital autoradiography was performed using the α-camera (*32*) to visualize the activity and its distribution at subtissue levels. After administration of ^{225}Ac-L1 (0.4 MBq) via tail-vein injection, the mice were sacrificed at 2 and 24 h ($n = 2$) (experiment 5). Kidneys, salivary glands, and tumors were harvested and immediately embedded in optimal-cutting-temperature compound, frozen on dry ice, and cryostat-sectioned in 8-μm sections. Image analysis was performed using ImageJ Fiji (version 1.49g; National Institutes of Health). The relative ^{225}Ac-L1 activity concentrations at the subtissue level versus the average of the whole tissue sample were calculated.

RPT

Efficacy in a Flank Xenograft Model. Mice were injected subcutaneously within the flank with 2×10^6 PSMA+ PC3 PIP or 1×10^6 PSMA− PC3 flu cells. Treatments (^{213}Bi-L1 and ^{225}Ac-L1, experiments 6–7) were conducted 12–15 d later when tumor volume was less than 100–150 mm^3. Tumors were then measured 2–3 times per week until they reached 1,000 mm^3. Three mice from each group ($n = 3$ per group) were removed to evaluate acute toxicity after 8 wk.

Efficacy in a Micrometastatic Model. PC3-ML-fLuc-PSMA cells were maintained as described previously (*21*). Briefly, mice were injected intravenously with 1×10^6 PC3-ML-fLuc-PSMA cells

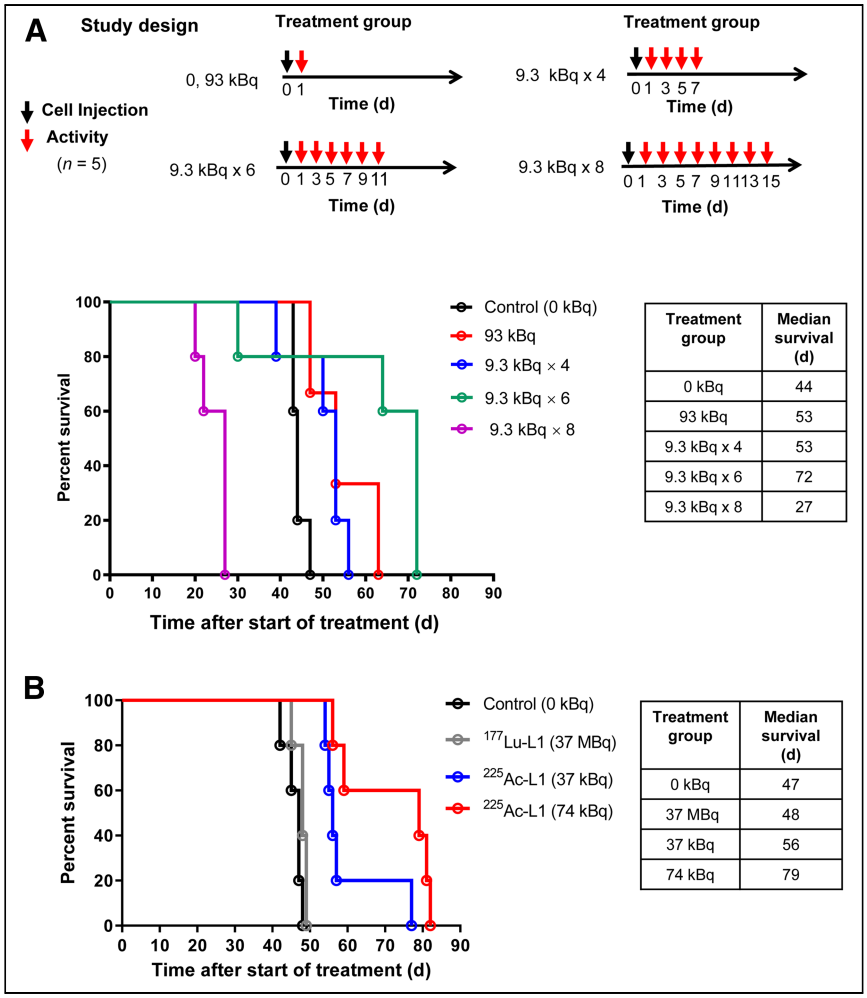

FIGURE 4. Treatment effect in PSMA+ micrometastatic model. (A) Study design and Kaplan–Meier curve showing activity-dependent survival benefit after single and multiple administrations. (B) Kaplan–Meier curve showing improved survival after single administration of ^{225}Ac-L1 compared with ^{117}Lu-L1.

(experiment 8A). One day later, mice were injected intravenously with 93 kBq of ^{225}Ac-L1 (group 1) and with the fractionated activity of 9.3 kBq at a 48-h interval (group 2 [×4], group 3 [×6], group 4 [×8], and control group [0 kBq]). Metastatic tumor progression was monitored by in vivo bioluminescence imaging (IVIS Spectrum; Perkin-Elmer) and survival. A second study was performed on a micrometastatic model (experiment 8B) using ^{225}Ac-L1 (37 and 74 kBq) and ^{177}Lu-L1 (37 MBq) and a control group (0 kBq).

Toxicity and Maximum Tolerated Activity (MTA). The MTA was defined as the highest activity at which no animal died or lost more than 20% of its pretreatment weight. Mice (body weight, 34.9 ± 0.5 g) were weighed and inspected twice per wk for at least 12 mo. A toxicity study was also performed using the fractionated activity scheme applied for the micrometastatic model (0 kBq, 93 kBq, 9.3 kBq × 4, 9.3 kBq × 6, and 9.3 kBq × 8) (experiment 9). A separate study (experiment 10) was also performed, in which we administered ^{225}Ac-L1 intravenously at doses of 18.5 kBq × 2 (group 1) and 37 kBq × 2 (group 2)—doses that were based on the activity used for the treatment of the flank tumor model. The control group (group 3) received only saline vehicle. On sacrifice, animals were evaluated by the Johns Hopkins Phenotyping Core. Complete blood count, serum chemistry, necropsy, and histopathology (>30 tissues) were performed. Urinalysis (Chemstrip Test Strips; Roche Diagnostics) for specific gravity and protein was performed monthly for each animal.

Statistical Analysis

Statistical significance was calculated using an unpaired 2-tailed *t* test. Kaplan–Meier curves were analyzed, and survival was compared, using the log-rank test.

RESULTS

Radiolabeling

We developed a fast microwave-assisted radiolabeling method to synthesize ^{213}Bi-L1 and ^{225}Ac-L1 with high yield (>90% [decay corrected]) and purity (>98%) and with molar activity higher than 8.9 MBq/nmol. The HPLC method also enabled separation of ^{213}Bi-L1 from ^{225}Ac-L1 and the excess ligand because of their different retention times. ^{213}Bi-L1 is assumed to be generated from starting ^{225}Ac$(NO_3)_3$ that had ^{213}Bi as the decay product. Because actinium has no stable isotope, we have evaluated several conventional surrogates—Bi-L1, La-L1, and Lu-L1—as reference compounds for HPLC (Supplemental Figs. 1–3). ^{225}Ac-L1 demonstrated a longer retention time than those surrogate compounds. PSMA binding affinities of stable analogs ranged from 0.1–5.1 nM. *In cellula* experiments demonstrated high and specific cell uptake and killing efficiency for both ^{213}Bi-L1 and ^{225}Ac-L1 in PSMA+ PC3 PIP cells (Fig. 1B). PSMA− PC3 flu cells were insensitive to either compound under similar conditions. ^{225}Ac-L1 (A_0, 9–12 kBq/mL) was more effective than ^{213}Bi-L1 (95–122 kBq/mL) in PSMA+ cells (Fig. 1B).

Biodistribution

The biodistribution of ^{213}Bi-L1 (Fig. 2A, experiment 1) was determined up to 2 h, considering its short half-life. PSMA+ PC3 PIP tumor uptake was high as early as 10 min after injection (18.9 ± 3.1 %ID/g) and increased at 2 h (29.4 ± 8.0 %ID/g). The agent displayed rapid clearance from blood, showing a drop from 5.1 ± 1.7 %ID/g at 10 min to 0.57 ± 0.0 %ID/g at 2 h. Renal uptake was 49.0 ± 21.2 %ID/g at 10 min and cleared rapidly to 23.1 ± 6.7, 9.9 ± 1.8, and 8.6 ± 3.0 %ID/g at 30 min, 1 h, and 2 h, respectively. Activity in the heart, liver, spleen, and salivary glands was less than 1 %ID/g after 2 h.

The biodistribution of ^{225}Ac-L1 was determined up to 8 d after administration (Fig. 2A, experiment 2). ^{225}Ac-L1 cleared rapidly from the blood pool (<0.5 %ID/g at all time points) and efficiently accumulated in the PSMA+ tumor to 45.8 ± 17.9 %ID/g at 2 h and 44.5 ± 12.9 %ID/g at 8 h, remaining high, at 49.0 ± 17.9 %ID/g, at 24 h. Clearance from tumor was protracted, at 22.0 ± 7.5 %ID/g at

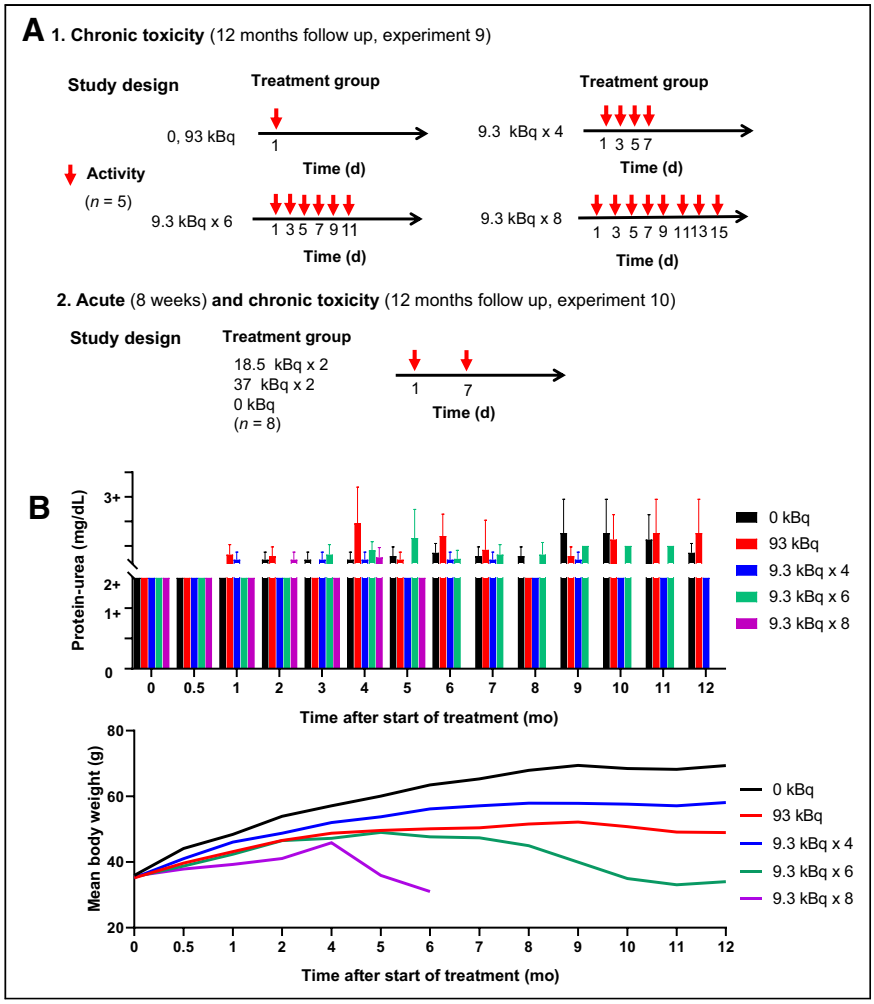

FIGURE 5. (A) Study design (1 and 2) of the chronic and acute toxicity studies performed using immunocompetent CD-1 mice. (B) Analysis of radiotoxicity parameters of ^{225}Ac-L1 in healthy CD-1 mice (n = 5) for 1–12 mo. Measured urine protein level by dipstick showed activity-dependent proteinuria occurring in treatment groups (top). Urine protein (trace, 0–10 mg/dL; 1+, 30 mg/dL; 2+, 100 mg/dL, 3+, 300 mg/dL) and mean body weight (bottom).

48 h, 18.3 ± 4.1 %ID/g at 72 h, 19.2 ± 6.4 %ID/g at 96 h, 12.6 ± 3.2 %ID/g at 120 h, and 10.0 ± 2.2 %ID/g at 8 d. Renal uptake was highest at 2 h, at 27.5 ± 14.9 %ID/g, followed by relatively rapid clearance to 3.1 ± 0.9 %ID/g at 8 h and 1.5 ± 0.5 %ID/g at 24 h and dropping below 1% at later times. Tumor-to-kidney ratios increased from 79.3 ± 25.0 at 2 h to 314.5 ± 185.8 at 8 h, 203.8 ± 123.1 at 24 h, 101.0 ± 64.3 at 48 h, 242.5 ± 107.8 at 72 h, 168.7 ± 33.5 at 96 h, 147.9 ± 40.2 at 120 h, and 148 ± 75 at 8 d. Biodistribution beyond 8 d was not determined because of a significant reduction in PSMA+ tumor volume.

Among normal organs, liver displayed moderate uptake at 8 h (3.9 ± 1.1 %ID/g) and remained at that level at 24 h (3.1 ± 0.8 %ID/g), decreasing to 2.1 ± 0.4 %ID/g at 8 d after injection. Accordingly, a biodistribution study was performed on tumor-free CD-1 mice to determine whether liver retention was related to the animal model or whether ^{225}Ac-L1 was chemically unstable in vivo (experiment 4). Our previous studies revealed significantly higher liver uptake in immunodeficient tumor-bearing NSG mice than in immunocompetent CD-1 mice when administered with the anti-PSMA antibody ^{111}In-5D3 (*33*). Consistent with the previous report, ^{225}Ac-L1 also displayed significantly lower liver uptake (≤1 %ID/g) at all time points in CD-1 mice. Blood and all other normal tissues showed low uptake (<1%) after 8 h.

Morphologic changes in the tissues were evaluated by H&E staining (Fig. 2B). Whole-tumor H&E staining at 96 h and 8 d displayed necrosis within the treated tumors. PSMA immunohistochemical staining within the PSMA+ PC3 PIP tumors revealed a decrease in PSMA expression at 24–192 h compared with tumor harvested from control animals that did not receive radioactivity. This decrease could be attributed to a treatment effect that resulted in a decrease in PSMA+ tumor cells with time.

RPT

Antitumor Effect in the Flank Tumor Model. The study design and activity-dependent treatment effects of ^{225}Ac-L1 in this model are shown in Figure 3 (experiment 7). The control groups (untreated PSMA+ or PSMA− and the PSMA− tumor-bearing group with 18.5 kBq × 2) did not show any significant difference in the time to reach a 10-fold increase in tumor volume (V_t) from the initial tumor volume (V_0) ($V_t/V_0 \leq 10$), with a median survival of 17 d. Animals receiving any single dose or 2 fractionated doses (7 d apart) demonstrated a significant tumor growth delay in PSMA+ tumors ($P < 0.003$) compared with the control groups. However, slow tumor regrowth was observed after 8 wk in the treatment groups that received 9.3 kBq × 1 and 9.3 kBq × 2 doses. In contrast, a durable treatment effect was seen when PSMA+ PIP-bearing animals received 18.5 kBq × 2 (Fig. 3B), where median $V_t/V_0 \leq 10$ was 168 d. Significantly, whereas the single administration of 18.5 kBq resulted in an increase in $V_t/V_0 > 10$ within 8 wk for 3 mice from this group, the remaining 2 mice displayed significant tumor growth control and increased body-weight recovery indicating relatively lower radiotoxicity than in the rest of the treated groups. The median time to reach a $V_t/V_0 \leq 10$ is listed in Figure 3B. A preliminary efficacy study was also performed with ^{213}Bi-L1 (3.7 MBq). It showed expected tumor control ($V_t/V_0 \leq 10$ [35 d]) compared with the untreated group (15 d) (Supplemental Fig. 4) in the PSMA+ flank tumor model.

Antitumor Effect in the PSMA+ Micrometastatic Model. The study design and efficacy of ^{225}Ac-L1 as single and fractionated activity are shown in Figure 4A (experiment 8A). Mice that received 9.3 kBq × 6 of ^{225}Ac-L1 demonstrated the highest survival ($P <$ 0.002), with a median survival of 72 d, compared with 44 d for the untreated group, from initiation of the experiment.

A separate experiment was performed to compare the effect of a single administration of ^{225}Ac-L1 with that of ^{177}Lu-L1 (37 MBq)

(Fig. 4B, experiment 8B). No survival benefit for the group treated with ^{177}Lu-L1 was observed compared with the untreated group, with median survival times of 46 and 47 d, respectively. In contrast, ^{225}Ac-L1 (37 and 74 kBq) displayed significantly increased survival over controls ($P < 0.001$).

In Vivo Radiotoxicity and MTA. The designs of the chronic and acute toxicity studies are shown in Figures 5A and 5B (experiments 9–10). Acute toxicity of ^{225}Ac-L1 was evaluated in tumor-bearing NSG mice after 8 wk and in tumor-free CD-1 mice. In general, blood counts and chemistry (Supplemental Tables 6–7) were not significantly affected, acutely, compared with untreated control mice.

A chronic toxicity study was performed by following the fractionated dosage scheme (Fig. 5A) used for the micrometastatic model, which assessed the long-term effects of ^{225}Ac-L1 (Fig. 5B; Supplemental Table 8). All mice treated with 93 kBq ($n = 5/5$) and 9.3 kBq × 4 survived for over 12 mo. Significantly, all treated mice displayed acceptable hematologic changes compared with the untreated mice. Moderate changes in creatinine and blood urea alanine levels (for kidney function) were seen only for the higher-treatment groups, with renal cortical changes (H&E) not seen in the control group (Supplemental Fig. 6). Elevated values of aspartate aminotransferase, alanine aminotransferase, and γ-glutamyl transferase were consistent with liver toxicity in these 2 groups.

Limited chronic toxicity testing was also performed applying the activity used for flank tumor models (experiment 10). Although 3 of 5 CD-1 mice treated with 18.5 kBq × 2 survived after 12 mo (Supplemental Table 9), the group treated with 37 kBq × 2 showed significant weight loss after 6 mo. All mice from that latter group were removed from the study to evaluate the activity-limiting toxicity. Elevated aspartate aminotransferase, alanine aminotransferase, and γ-glutamyl transferase were consistent with liver damage in treated animals, as seen from experiment 9. The parotid glands displayed smaller acini and higher cytoplasmic variation after 1 y in mice treated with 18.5 kBq × 2 than in controls (Supplemental Fig. 7). There were more cytoplasmic variation and anisocytosis in the lacrimal gland tissue in 2 treated mice.

In summary, on the basis of the chronic toxicity studies, MTA was conservatively determined as the fractionated administration of 9.3 kBq × 4. The fractionated dosage of 18.5 kBq × 2 may also be considered safe. Two mice that died at month 10–11 were not available for pathologic assessment. Lung tumors smaller than 5 mm in diameter were identified in 2 treated animals from the chronic toxicity studies. Such spontaneous tumorigenesis (adenoma of lung and liver) is the common cause of death for older CD-1 mice (*34*,*35*).

α-Camera Imaging and Dosimetry

Figures 6A and 6B provide a selected list of the murine ADCs. PSMA+ PC3 PIP tumors received the highest ADC (680 mGy/kBq), followed by liver (94 mGy/kBq) and kidney (82 mGy/kBq). The doses absorbed by other normal tissues were low. Therapeutic PSMA+ tumor–to–normal-organ ratios were calculated for selected organs (Fig. 6B). Therapeutic ratios were high and followed the order bone marrow (1,115) >> salivary gland (123) > blood (40) > kidney (8.3) and liver (7.2), indicating either kidney or liver as the absorbed dose–limiting organ. Estimated human average organ ADCs from OLINDA/EXM, based on mouse-to-human time-integrated activity conversion for selected organs, are listed in Supplemental Table 5.

The distribution of radioactivity within the tumor, kidney, and salivary glands was further evaluated ex vivo by α-camera imaging at 2 and 24 h after treatment (Fig. 6C, experiment 5). The kidney displayed a highly heterogeneous intraorgan distribution of radioactivity, with preferential renal cortical accumulation as anticipated from the high levels of PSMA within this region (*36*) and the accumulation of free ^{213}Bi (*37*). Rapid clearance of ^{225}Ac was observed after 24 h, consistent with the biodistribution data and further reflecting the favorable pharmacokinetics of ^{225}Ac-L1. The ratio of signal intensity within the renal cortex to that within the medulla was 4:1 at 2 h. A uniform distribution of radioactivity was noted in PSMA+ tumor at both time points, indicating sufficient internalization of ^{225}Ac after 24 h to produce an antitumor effect. A nonuniform distribution of radioactivity within the salivary glands was found for both parotid and submandibular glands at 2 h, with radioactivity levels too low to enable imaging at 24 h.

DISCUSSION

PSMA α-RPT holds great potential as a safe and effective treatment option for patients with mCRPC. Although α-RPT with ^{225}Ac-PSMA-617 has demonstrated substantial responses, salivary gland radiotoxicity has curtailed widespread adoption of this agent (*20*). Here, we report a detailed preclinical investigation of a new ^{225}Ac-labeled compound, with attention to radiolabeling method, biodistribution, efficacy in 2 human tumor models, radiotoxicity, and α-camera–guided dosimetry. The goal was to provide an ^{225}Ac-labeled compound that might be as effective as, or more effective than, existing agents but with fewer off-target effects.

Since the initial demonstration of ^{213}Bi-labeled and, more recently, ^{227}Th-labeled anti-PSMA antibodies for α-RPT (*38*,*39*), several low-molecular-weight PSMA α-RPTs have been developed preclinically for their fast and favorable pharmacokinetics as demonstrated clinically by ^{225}Ac-PSMA-617 (*14*). Unconventional radioisotopes to enable concurrent PET imaging (*40*) or efforts to improve the therapeutic window, often at the expense of increased retention in the blood (*23*), have been pursued. Studies are also directed toward developing a more relevant tumor model to address PSMA heterogeneity, which has been demonstrated in the clinical setting (*41*). It is challenging to compare the safety and efficacy of those reported compounds with ^{225}Ac-L1 because of the different tumor models and murine species involved and the lack of readily available long-term toxicity data in the literature. We did not perform detailed safety and efficacy studies for ^{213}Bi-L1 because of the inconveniently short half-life of ^{213}Bi and the sense that if we were to move forward clinically, it would be with ^{225}Ac-L1 or a close analog.

There are several key outcomes from this work. First, we presented an optimized radiosynthesis method to provide the highest possible molar specific activity for ^{225}Ac-L1. Second, we used biodistribution studies together with α-camera–guided dosimetry to uncover the dose-limiting organ, which could be kidney or liver and, less likely, bone marrow. The data were supported by long-term radiotoxicity studies, which revealed that the liver and—less likely—kidney were the dose-limiting organs. Notably, whereas a high single dose of ^{177}Lu-L1 (111 MBq) did not generate renal or hematologic toxicity after 1 y of follow-up (*24*), ^{225}Ac-L1 indeed displayed typical renal cortical damage at the higher doses; 4 × 9.3 kBq was considered the MTA. Third, consistent with our previous report on ^{212}Pb-based α-RPT (*15*), the data also revealed superior efficacy of α-RPT compared with β-RPT (^{177}Lu-L1) in treating micrometastatic disease. Considering the energy ratio of ^{225}Ac (27 MBq) to ^{177}Lu (0.4 MBq) of 70 to 1,

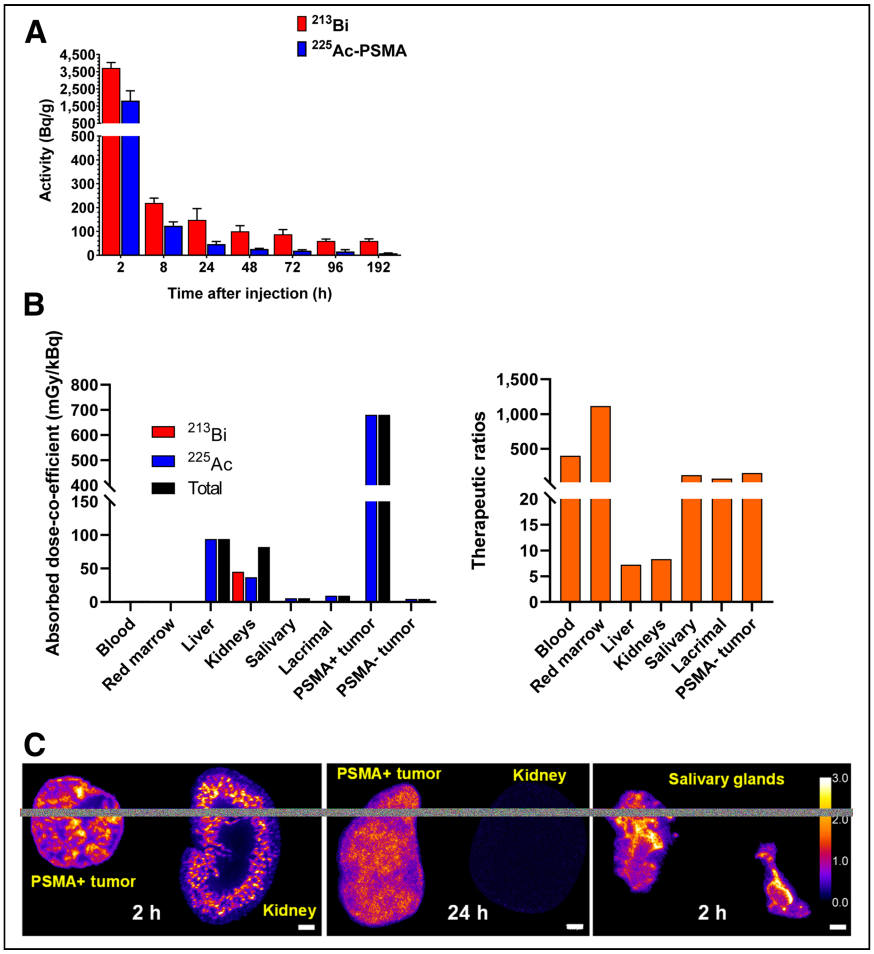

FIGURE 6. (A) Activity per unit mass (Bq/g) within kidneys of free in vivo–generated ^{213}Bi and equilibrium ^{225}Ac-L1. (B) ADC of selected tissues and therapeutic ratio (ADC of PSMA+ tumor–to–normal-organ ratio). (C) α-camera images showing suborgan activity distribution within kidney and in tumor (significant renal cortical clearance was observed after 24 h) (left and middle) and α-camera image of submandibular and parotid salivary glands (right). Scale indicates activity concentration normalized with average activity in tumor at 2 h (left), in tumor at 24 h (middle), and in salivary glands at 2 h (right). α-camera exposure is 30 min (left and middle) and 24 h (right).

^{225}Ac-L1 (4 × 9.3 kBq) demonstrated an approximately 10- to 12-d survival benefit using a safe dose at the MTA compared with ^{177}Lu-L1 (37 MBq). The administered dose of ^{177}Lu-L1 was 14-fold higher than that of ^{225}Ac-L1. Notably, a short half-life ^{211}At-labeled compound displayed significantly higher survival benefit than ^{225}Ac-L1, although long-term toxicity data revealed severe renal cortical damage at more than 10 mo after treatment (*21*). That finding underlines the potential advantage of ^{225}Ac α-RPT, even with concerns related to its α-emitting daughters. Fifth, low tumor-to-liver ratios were found for ^{225}Ac-L1, which we believe are most likely associated with immunocompromised NSG mice combined with the release of decayed daughters within the liver. Mild hepatobiliary radiotoxicity was also identified in long-term toxicity with higher doses of ^{225}Ac-L1 but not with ^{177}Lu-L1.

Human MTAs based on whole-organ dosimetry are 140 MBq for the liver as the dose-limiting organ and 130 MBq for the kidney, assuming a global relative biological effect of 5 relative to external-beam thresholds in units of a 2-Gy-fraction-equivalent of external-beam radiation (Supplemental Table 5C). However, liver dosimetry included all daughters from the ^{225}Ac decay chain, which is undoubtedly an overestimation of the absorbed dose because the liver is the likely source of the free daughters (^{221}Fr and ^{213}Bi) seen to accumulate in the kidney. Conversely, the kidney absorbed dose is likely underestimated in terms of toxicity threshold assessment because the activity was localized to portions of the cortex, most likely within the proximal tubules, based on α-camera imaging. A full dosimetric analysis of these and the value of suborgan relative biological effect representing the radiobiologic effects of α-particles is beyond the scope of this article. Regardless, projections of activity limits to humans from the murine studies are highly uncertain, and any clinical application should be performed in dose increments from values well below the calculated MTA.

We recognize that the high levels of PSMA in the PSMA+ PC3 PIP tumor xenograft present an unnatural situation—a limitation of our studies. A recent report by Current et al. using variable ratios of PSMA+ PC3 PIP with PSMA− PC3 flu cells might address that issue (*41*). On the basis of the data of Current et al., the efficacy of PSMA α-RPT correlates positively with the PSMA expression per cell and the fraction of PSMA+ cells per lesion. The number of PSMA receptors per PC3 PIP cell was measured to be approximately 5.5×10^5 (flow cytometry). On the basis of our study, ^{225}Ac-L1 could provide a curative dose of 50 Gy for the PSMA+ PC3 PIP tumor with an estimated dose of 31 MBq (Supplemental Table 5C). Additionally, our preclinical long-term toxicity study (extrapolated from a 35-g mouse to a 73.7-kg male adult human) revealed that the MTA for a male adult human is estimated to be about 77 MBq. Accordingly, approximately 2.2×10^5 PSMA receptors per cell would be treated safely using ^{225}Ac-L1 as a standalone therapy and is within the range of PSMA expression in the human prostate cancer cell lines C4-2 (*41*) and LNCaP (*42*).

Another limitation of our study is the use of a small number of control animals for toxicity studies. That situation was associated with the unexpected death of the treated mice during the 1-y-long toxicity studies, with matched control mice sacrificed to enable comparison of radiotoxicity. Such long-term radiotoxicity studies with more control animals will be important to initiate clinical translation of the studied α-RPT agents.

CONCLUSION

We have evaluated the new PSMA-based α-RPT agents ^{213}Bi-L1 and ^{225}Ac-L1. ^{225}Ac-L1 demonstrated a PSMA-specific tumor growth delay in both large and micrometastatic tumor models without causing off-target toxicity using fractionated activity administration. The results suggest testing ^{225}Ac-L1 in patients with mCRPC.

DISCLOSURE

Financial support was received from the Patrick C. Walsh Prostate Cancer Research Fund, EB024495, CA184228, and the Commonwealth Foundation. Sangeeta Ray, Il Minn, Ronnie Mease, and Martin Pomper are coinventors on one or more U.S. patents covering compounds discussed in this submission and, as such, are entitled to a portion of any licensing fees and royalties generated by this technology. This arrangement has been reviewed and approved by the Johns Hopkins University, following its conflict-of-interest policies. No other potential conflict of interest relevant to this article was reported.

ACKNOWLEDGMENTS

^{225}Ac, ^{212}Bi, and ^{177}Lu for this work were supplied by the U.S. Department of Energy Office of Science by the Isotope Program in the Office of Nuclear Physics. We thank Dr. Michael McDevitt for his valuable suggestion on an experiment.

KEY POINTS

QUESTION: Can we deliver PSMA-targeted α-RPT using ^{225}Ac-labeled low-molecular-weight radioligands to tumor-bearing mice safely and effectively?

PERTINENT FINDINGS: We investigated an optimized ^{225}Ac-labeled PSMA-targeted compound,^{225}Ac-L1, which safely demonstrated tumor growth control in both flank and micrometastatic models and did so more effectively than the corresponding ^{177}Lu-labeled analog. Our data indicate that it is possible to provide a safe and therapeutically effective dose of ^{225}Ac-L1.

IMPLICATIONS FOR PATIENT CARE: ^{225}Ac-L1, designed to mitigate off-target effects, is a promising candidate for clinical PSMA-targeted α-RPT.

REFERENCES

1. Key statistics for prostate cancer. American Cancer Society website. https://www.cancer.org/cancer/prostate-cancer/about/key-statistics.html. Revised January 12, 2021. Accessed February 8, 2021.
2. Silver DA, Pellicer I, Fair WR, Heston WD, Cordon-Cardo C. Prostate-specific membrane antigen expression in normal and malignant human tissues. *Clin Cancer Res.* 1997;3:81–85.
3. Sweat SD, Pacelli A, Murphy GP, Bostwick DG. Prostate-specific membrane antigen expression is greatest in prostate adenocarcinoma and lymph node metastases. *Urology.* 1998;52:637–640.
4. Haberkorn U, Eder M, Kopka K, Babich JW, Eisenhut M. New strategies in prostate cancer: prostate-specific membrane antigen (PSMA) ligands for diagnosis and therapy. *Clin Cancer Res.* 2016;22:9–15.
5. Kiess AP, Banerjee SR, Mease RC, et al. Prostate-specific membrane antigen as a target for cancer imaging and therapy. *Q J Nucl Med Mol Imaging.* 2015;59:241–268.
6. Morris M, Vogelzang NJ, Sartor O, et al. Phase 1 study of the PSMA-targeted small-molecule drug conjugate EC1169 in patients with metastatic castrate-resistant prostate cancer (mCRPC) [abstract]. *Ann Oncol.* 2017;28(suppl):793PD.
7. Rahbar K, Ahmadzadehfar H, Kratochwil C, et al. German multicenter study investigating ^{177}Lu-PSMA-617 radioligand therapy in advanced prostate cancer patients. *J Nucl Med.* 2017;58:85–90.
8. Hofman MS, Violet J, Hicks RJ, et al. ^{177}Lu-PSMA-617 radionuclide treatment in patients with metastatic castration-resistant prostate cancer (LuPSMA trial): a single-centre, single-arm, phase 2 study. *Lancet Oncol.* 2018;19:825–833.
9. Hofman MS, Lawrentschuk N, Francis RJ, et al. Prostate-specific membrane antigen PET-CT in patients with high-risk prostate cancer before curative-intent surgery or radiotherapy (proPSMA): a prospective, randomised, multicentre study. *Lancet.* 2020;395:1208–1216.
10. Herrmann K, Schwaiger M, Lewis JS, et al. Radiotheranostics: a roadmap for future development. *Lancet Oncol.* 2020;21:e146–e15.
11. Kassis AI. Therapeutic radionuclides: biophysical and radiobiologic principles. *Semin Nucl Med.* 2008;38:358–366.
12. Rathke H, Flechsig P, Mier W, et al. Dosimetry estimate and initial clinical experience with ^{90}Y-PSMA-617. *J Nucl Med.* 2019;60:806–811.
13. Zechmann CM, Afshar-Oromieh A, Armor T, et al. Radiation dosimetry and first therapy results with a $^{124I/131}$I-labeled small molecule (MIP-1095) targeting PSMA for prostate cancer therapy. *Eur J Nucl Med Mol Imaging.* 2014;41:1280–1292.
14. Kratochwil C, Bruchertseifer F, Rathke H, et al. Targeted α-therapy of metastatic castration-resistant prostate cancer with 225Ac-PSMA-617: dosimetry estimate and empiric dose finding. *J Nucl Med.* 2017;58:1624–1631.
15. Banerjee SR, Minn I, Kumar V, et al. Preclinical evaluation of $^{203/212}$Pb-labeled low-molecular-weight compounds for targeted radiopharmaceutical therapy of prostate cancer. *J Nucl Med.* 2020;61:80–88.
16. Sathekge M, Bruchertseifer F, Vorster M, et al. Predictors of overall and disease-free survival in metastatic castration-resistant prostate cancer patients receiving ^{225}Ac-PSMA-617 radioligand therapy. *J Nucl Med.* 2020;61:62–69.
17. Scheinberg DA, McDevitt MR. Actinium-225 in targeted alpha-particle therapeutic applications. *Curr Radiopharm.* 2011;4:306–320.
18. Morgenstern A, Apostolidis C, Kratochwil C, Sathekge M, Krolicki L, Bruchertseifer F. An overview of targeted alpha therapy with ^{225}actinium and ^{213}bismuth. *Curr Radiopharm.* 2018;11:200–208.
19. Song H, Hobbs RF, Vajravelu R, et al. Radioimmunotherapy of breast cancer metastases with alpha-particle emitter ^{225}Ac: comparing efficacy with ^{213}Bi and ^{90}Y. *Cancer Res.* 2009;69:8941–8948.
20. Langbein T, Chaussé G, Baum RP. Salivary gland toxicity of PSMA radioligand therapy: relevance and preventive strategies. *J Nucl Med.* 2018;59:1172–1173.
21. Kiess AP, Minn I, Vaidyanathan G, et al. (2*S*)-2-(3-(1-carboxy-5-(4-^{211}At-astatobenzamido)pentyl)ureido)-pentanedioic acid for PSMA-targeted α-particle radiopharmaceutical therapy. *J Nucl Med.* 2016;57:1569–1575.
22. Nonnekens J, Chatalic KL, Molkenboer-Kuenen JD, et al. ^{213}Bi-labeled prostate-specific membrane antigen-targeting agents induce DNA double-strand breaks in prostate cancer xenografts. *Cancer Biother Radiopharm.* 2017;32:67–73.
23. Kelly JM, Amor-Coarasa A, Ponnala S, et al. A single dose of ^{225}Ac-RPS-074 induces a complete tumor response in an LNCaP xenograft model. *J Nucl Med.* 2019;60:649–655.
24. Banerjee SR, Kumar V, Lisok A, et al. ^{177}Lu-labeled low-molecular-weight agents for PSMA-targeted radiopharmaceutical therapy. *Eur J Nucl Med Mol Imaging.* 2019;46:2545–2557.
25. Banerjee SR, Pullambhatla M, Byun Y, et al. Sequential SPECT and optical imaging of experimental models of prostate cancer with a dual modality inhibitor of the prostate-specific membrane antigen. *Angew Chem Int Ed Engl.* 2011;50:9167–9170.
26. Ray Banerjee S, Chen Z, Pullambhatla M, et al. Preclinical comparative study of ^{68}Ga-labeled DOTA, NOTA, and HBED-CC chelated radiotracers for targeting PSMA. *Bioconjug Chem.* 2016;27:1447–1455.
27. Olszewski RT, Bukhari N, Zhou J, et al. NAAG peptidase inhibition reduces locomotor activity and some stereotypes in the PCP model of schizophrenia via group II mGluR. *J Neurochem.* 2004;89:876–885.
28. Franken NAP, Rodermond HM, Stap J, Haveman J, van Bree C. Clonogenic assay of cells in vitro. *Nat Protoc.* 2006;1:2315–2319.
29. Bolch WE, Eckerman KF, Sgouros G, Thomas SR. MIRD pamphlet no. 21: a generalized schema for radiopharmaceutical dosimetry—standardization of nomenclature. *J Nucl Med.* 2009;50:477–484.
30. Josefsson A, Nedrow JR, Park S, et al. Imaging, biodistribution, and dosimetry of radionuclide-labeled PD-L1 antibody in an immunocompetent mouse model of breast cancer. *Cancer Res.* 2016;76:472–479.
31. Stabin MG, Sparks RB, Crowe E. OLINDA/EXM: the second-generation personal computer software for internal dose assessment in nuclear medicine. *J Nucl Med.* 2005;46:1023–1027.
32. Bäck T, Jacobsson L. The α-camera: a quantitative digital autoradiography technique using a charge-coupled device for ex vivo high-resolution bioimaging of α-particles. *J Nucl Med.* 2010;51:1616–1623.
33. Banerjee SR, Kumar V, Lisok A, et al. Evaluation of 111In-DOTA-5D3, a surrogate SPECT imaging agent for radioimmunotherapy of prostate-specific membrane antigen. *J Nucl Med.* 2019;60:400–406.
34. Brayton CF, Treuting PM, Ward JM. Pathobiology of aging mice and GEM: background strains and experimental design. *Vet Pathol.* 2012;49:85–105.
35. Engelhardt JA, Gries CL, Long GG. Incidence of spontaneous neoplastic and nonneoplastic lesions in Charles River CD-1 mice varies with breeding origin. *Toxicol Pathol.* 1993;21:538–541.
36. Bacich DJ, Pinto JT, Tong WP, Heston WDW. Cloning, expression, genomic localization, and enzymatic activities of the mouse homolog of prostate-specific membrane antigen/NAALADase/folate hydrolase. *Mamm Genome.* 2001;12:117–123.

37. Miederer M, McDevitt MR, Sgouros G, Kramer K, Cheung N-KV, Scheinberg DA. Pharmacokinetics, dosimetry, and toxicity of the targetable atomic generator, ^{225}Ac-HuM195, in nonhuman primates. *J Nucl Med.* 2004;45:129–137.
38. McDevitt MR, Barendswaard E, Ma D, et al. An α-particle emitting antibody (^{213}Bi-J591) for radioimmunotherapy of prostate cancer. *Cancer Res.* 2000;60:6095–6100.
39. Hammer S, Hagemann UB, Zitzmann-Kolbe S, et al. Preclinical efficacy of a PSMA-targeted thorium-227 conjugate (PSMA-TTC), a targeted alpha therapy for prostate cancer. *Clin Cancer Res.* 2020;26:1985–1996.
40. Umbricht CA, Köster U, Bernhardt P, et al. Alpha-PET for prostate cancer: preclinical investigation using ^{149}Tb-PSMA-617. *Sci Rep.* 2019;9:17800.
41. Current K, Meyer C, Magyar CE, et al. Investigating PSMA-targeted radioligand therapy efficacy as a function of cellular PSMA levels and intra-tumoral PSMA heterogeneity. *Clin Cancer Res.* 2020;26:2946–2955.
42. Lückerath K, Stuparu AD, Wei L, et al. Detection threshold and reproducibility of ^{68}Ga-PSMA11 PET/CT in a mouse model of prostate cancer. *J Nucl Med.* 2018; 59:1392–1397.